DISTANCE PROTECTION ON MMC-HVDC TRANSMISSION LINES WITH SINGLE-ENDED MEASUREMENTS

Ruiyu Pan[1,2], Yu Liu[1*], Binglin Wang[1], and Xiaodong Zheng[3]

[1]School of Information Science and Technology, ShanghaiTech University, Shanghai, China
[2]Shanghai Engineering Research Center of Energy Efficient and Custom AI IC, Shanghai, China
[3] Key Laboratory of Control of Power Transmission and Conversion (Ministry of Education), Shanghai Jiao Tong University, Shanghai, China
**corresponding author: liuyu.shanghaitech@gmail.com, liuyu@shanghaitech.edu.cn*

Keywords: MMC-HVDC GRIDS, DISTANCE PROTECTION, TRANSMISSION LINE

Abstract

MMC-HVDC grid is a promising way to incorporate a large number of renewable generations. Protection of transmission lines is essential to guarantee the safe operation of the grid during line faults. However, the protection of MMC-HVDC lines requires very high operational speed (typically within 3ms), without losing dependability and security of the protection. This paper proposes a novel distance protection for MMC-HVDC transmission lines. The method only utilizes single-ended measurements, and no communication channels between line terminals are required. First, the model of the transmission line with fault is derived, with the line resistance and inductance "seen" by the relay as the unknown variables. Afterwards, the state estimation procedure is applied to accurately estimate the resistance/inductance. Finally, the trip signal and the faulted pole are determined by comparing the calculated resistance/inductance with the relay characteristics. Numerical experiments in PSCAD/EMTDC show that the proposed method can dependably operate during internal faults within 3ms after the occurrence of the fault, and securely ignore external faults. The calculation burden of the algorithm is small to enable real-time operation of the proposed distance protection method.

1 Introduction

With increasing demand for clean energy to reduce carbon emissions, large-scale renewable energy sources are connected to the practical power grids via high voltage direct current (HVDC) transmission lines [1-2]. Modular multilevel converter (MMC) has the advantages of high operating reliability, superior harmonic performance, high modularity and scalability [3-4]. Therefore, MMC-HVDC grids are promising candidates to integrate large amount of clean energy in future power systems. Protective relaying on transmission lines is important to guarantee the safety and reliable operation of the power grid [5-6]. The existing line protection functions in MMC-HVDC grids mainly include single-ended methods and double-ended methods.

Single-ended methods only utilize local terminal measurements and do not require communication channels. For the conventional methods such as differential under-voltage protection, the internal fault is detected when the voltage derivative is larger than a certain setting and the voltage is less than a threshold within a certain time window [7]. However, the method may encounter selectivity issues since external faults could also cause large change rate of the voltage. Single-ended travelling wave protection is widely adopted in practical systems. The single-ended travelling wave protections of ABB and SIEMENS are usually utilized as the main protections. The principle of ABB method is to detect the fault via derivative of reverse voltage traveling wave (polar wave). The principle of SIEMENS method is to adopt derivative of voltage and derivative of current polar wave for fault detection [8]. However, the two methods are based on the considerable transient component caused by the fault. Therefore, similar selectivity issues still exist since external faults may also cause large transient components. In order to improve the performance of traveling wave protection, several methods were proposed. Reference [9] introduced the traditional traveling-wave based direction criterion, and improved the protection criterion at the high frequency band to reduce the effect of frequency dependent characteristic. In [10], a Levenberg–Marquart (LM) optimal approximation method is proposed to extract the fault distance information from zero-sequence fault current initial traveling wave to improve the sensitivity of the protection.

To further overcome the selectivity issues, the boundary characteristic based methods were proposed [11-14]. Transmission line in MMC-HVDC grids is usually equipped with the boundary inductors at line terminals. The current will be attenuated after passing the inductors and this characteristic could help protection function to distinguish internal faults from external faults. In [11], the equivalent impedance is discontinuous and the traveling wave will experience a bounce phenomenon when passing through the boundary elements. In [12], a HVDC line boundary

This work is sponsored by National Nature Science Foundation of China (No. 51807119, No. 51877135). The support is greatly appreciated.

protection method based on the smoothing reactor and DC filters is proposed. In [13], a boundary protection scheme using the difference characteristics of high-frequency energy is studied. In [14], the authors used the wavelet transform to extract the high-frequency voltage to identify the internal and external faults.

Double-ended methods utilize dual terminal measurements with the proper communication channels. With the exchanged information from the dual terminals, the selectivity of the protection method could be ensured. The current differential protection verifies the Kirchhoff's Current Laws (KCLs) of the line. The internal fault is detected when the sum of the dual terminal currents is much larger than zero. However, the charging capacitive current on transmission lines in MMC-HVDC grids is extremely large during the system disturbance. To avoid mal-operation during external faults, current differential protection usually requires a long time delay. Therefore, the method can only work as a backup protection. To improve the performance of the current different protection, the Bergeron model is utilized to compensate the capacitive current [15], however, the method still requires time delay of tens milliseconds at least. The other dual-ended methods are also proposed in [16-19], including dual-ended traveling wave based methods, pilot directional comparison methods, dynamic state estimation based methods, etc. Above dual-ended methods require the reliable communication channels, and the protection operation speed may be affected by the communication delay.

Legacy distance protection has been widely applied in existing AC transmission lines. However, legacy distance protection cannot be applied directly to the MMC-HVDC transmission line due to the following reasons. (a) MMC-HVDC grids are without AC excitations at a fixed frequency, (b) It requires a long data window (typically one cycle) to calculate phasors and the impedance "seen" by the relay; (c) it cannot protect the entire length of the line due to selectivity issues at the remote end of the line. To solve above issues, a distance protection scheme is proposed in this paper. The method accurately estimates the resistance/inductance "seen" by the relay using instantaneous measurements at the local end, and is compatible with the characteristics of DC grids such as short data window and no AC excitations. In addition, since there exist boundary inductors at line terminals of the DC grids, the distance protection can be carefully designed such that the internal and external faults near the remote end can be clearly identified. The proposed distance protection method can achieve dependability and instantaneous trip during internal faults through the entire length of the DC transmission line within 3 ms, and secure operation during external faults.

The rest of the paper is arranged as follows. Section 2 introduces the methodology of the proposed distance protection on MMC-HVDC transmission lines. Section 3 verifies the proposed distance protection method via numerical experiments. Section 4 draws a conclusion.

2 Methodology

2.1 Line Protection Requirements in MMC-HVDC Grids

An example multi-terminal MMC-HVDC grid is shown in Fig. 1. In this figure, the line of interest is the dual-pole transmission line connecting MMC1 and MMC3. Current limiting inductors (boundary inductors) are installed at terminals of transmission lines, to limit the currents during faults. The protection system of the line needs to dependably trip the line during internal faults, and securely ignore all external faults and other system disturbances. Also, to ensure that the DC circuit breakers can interrupt the fault currents, the protection system should trip internal faults extremely fast (eg. Zhangbei project requires that the protection system issues trip signal within 3 ms after the occurrence of the fault).

To achieve this goal, this paper tries to propose a protection algorithm based on measurements at the local terminal of the line, and try to meet the aforementioned requirements of the protective relay. The available measurements include instantaneous voltages and currents of the positive pole and the negative pole at the local terminal, namely, $u_p(t)$, $i_p(t)$, $u_n(t)$, and $i_n(t)$, respectively.

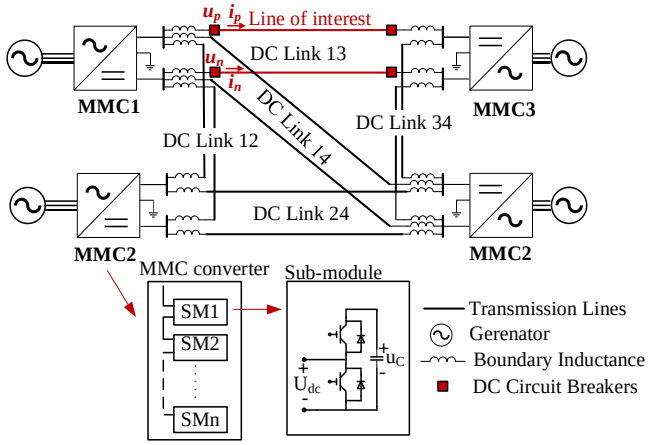

Fig. 1. An Example MMC-HVDC Grid

2.2 Relationship among Measured Voltages and Currents during Faults

To properly design a distance protection algorithm, next the relationship among voltage and current measurements at the local terminal during faults is carefully studied. To simplify the analysis, here the transmission line is modelled as a lumped RL model in the matrix form. During faults, the transmission line model is shown in Fig.2, where R_s and R_m are the self and mutual resistances of the line, L_s and L_m are the self and mutual inductances, $u_{fp}(t)$ and $u_{fn}(t)$ are the positive and negative pole voltages at the location of the fault.

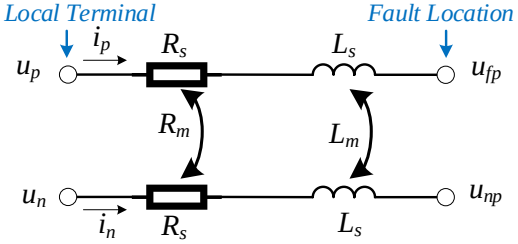

Fig. 2. Equivalent circuit of DC line during faults

From Fig. 2, the physical laws that the line should obey can be described via the following differential equation,

$$\begin{bmatrix} u_p(t) \\ u_n(t) \end{bmatrix} = \begin{bmatrix} R_s & R_m \\ R_m & R_s \end{bmatrix} \begin{bmatrix} i_p(t) \\ i_n(t) \end{bmatrix} + \begin{bmatrix} L_s & L_m \\ L_m & L_s \end{bmatrix} \frac{d}{dt} \begin{bmatrix} i_p(t) \\ i_n(t) \end{bmatrix} + \begin{bmatrix} u_{fp}(t) \\ u_{fn}(t) \end{bmatrix} \quad (1)$$

Note that the above equation holds for all types of faults. Next, the relationship is further simplified for each fault type.

2.2.1 Positive Pole to Ground Faults

During positive pole to ground (P-G) faults, assume that the positive pole voltage at the location of the fault is close to zero, i.e. $u_{fp}(t) = 0$. Therefore, from the first row of (1),

$$u_p(t) = R_s i_p(t) + R_m i_n(t) + L_s \frac{di_p(t)}{dt} + L_m \frac{di_n(t)}{dt} \quad (2)$$

Equation (2) could be rewritten as:

$$u_p(t) = R_1 \left[i_p(t) + k_R i_0(t) \right] + L_1 \left[\frac{di_p(t)}{dt} + k_L \frac{di_0(t)}{dt} \right] \quad (3)$$

where $R_1 = R_s - R_m$, $L_1 = L_s - L_m$, $k_R = R_m / R_1$, $k_L = L_m / L_1$, $i_0(t) = i_p(t) + i_n(t)$.

2.2.2 Negative Pole to Ground Faults

During negative pole to ground (N-G) faults, assume that the negative pole voltage at the location of the fault is close to zero, i.e. $u_{fn}(t) = 0$. Therefore, from the second row of (1),

$$u_n(t) = R_s i_n(t) + R_m i_p(t) + L_s \frac{di_n(t)}{dt} + L_m \frac{di_p(t)}{dt} \quad (4)$$

Equation (4) could be rewritten as:

$$u_n(t) = R_1 \left[i_n(t) + k_R i_0(t) \right] + L_1 \left[\frac{di_n(t)}{dt} + k_L \frac{di_0(t)}{dt} \right] \quad (5)$$

where the definitions of R_1, L_1, k_R, k_L, and $i_0(t)$ are consistent with those in (3).

2.2.3 Positive Pole to Negative Pole Faults

During positive pole to negative pole (P-N) faults, assume that the positive and negative pole voltages at the location of the fault are close to each other, i.e. $u_{fp}(t) = u_{fn}(t)$. Therefore, the difference between the first and the second row of (1) is,

$$u_p(t) - u_n(t) = R_1 \left[i_p(t) - i_n(t) \right] + L_1 \left[\frac{di_p(t)}{dt} - \frac{di_n(t)}{dt} \right] \quad (6)$$

where the definitions of R_1 and L_1 are consistent with those in (3).

In fact, since P-N faults are symmetrical faults, considering the DC system is symmetrical (the summation of the positive pole voltage and the negative pole voltage is zero), the voltage at the location of the fault should be zero, i.e. $u_{fp}(t) = u_{fn}(t) = 0$. In this case, equations (3) and (5) are also satisfied for P-N faults.

2.2.4 Positive Pole to Negative Pole to Ground Faults

During positive pole to negative pole to ground (PNG) faults, assume that both the positive and negative pole voltages at the location of the fault are close to zero, i.e. $u_{fp}(t) = u_{fn}(t) = 0$. Therefore, in this case equations (3), (5) and (6) are all satisfied.

2.3 Design of the Distance Protective Relay

The idea of legacy distance relay in AC system is to calculate the impedance "seen" by the relay. An internal fault is detected if the impedance "seen" by the relay is smaller than the impedance corresponding to the entire length of the line (or more generally speaking, falling into the trip region of the distance relay). The relay works for different types of faults, and can help identify the fault type.

Similarly, here a time domain distance relay in DC system is designed. From the analysis in section 2.2, the distance relay in this DC system should satisfy the following conditions: (a) the relay should be able to calculate the resistance and inductance "seen" by the relay, for different types of faults; (b) an internal fault is detected if the resistance and inductance "seen" by the relay enters a certain trip region; and (c) the distance relay should be able to identify the fault type, to ensure single pole tripping during single pole to ground faults.

In fact, one can observe from equations (3), (5) and (6) that they have the similar format, i.e.,

$$u_{cal}(t) = R_1 i_{cal}(t) + L_1 \frac{di_{cal}(t)}{dt} \quad (7)$$

where the values of $u_{cal}(t)$ and $i_{cal}(t)$ in (7) should be selected according to different fault types. In addition, the values of the differential term $di_{cal}(t)/dt$ should be numerically calculated for protection usage (here the central difference scheme is applied). The way of calculating $u_{cal}(t)$, $i_{cal}(t)$ and $di_{cal}(t)/dt$ are summarized in Table 1. Note that the difference between the positive and negative pole currents is known as the "difference mode" current in DC transmission lines. Here we refer to it as "mode 1".

2.3.1 Calculation of Resistance/Inductance Seen by the Relay

Next, the way of calculating the resistance and inductance seen by the relay is introduced. The key issue is to estimate R_1 and L_1 from available measurements $u_{cal}(t)$, $i_{cal}(t)$ and

Table 1. Selection of Voltages and Currents for Resistance/Inductance Estimation

	$i_{cal}(t)$	$u_{cal}(t)$	$di_{cal}(t)/dt$
Positive	$i_p(t) + k_R i_0(t)$	$u_p(t)$	$\frac{[i_p(t+\Delta t) - i_p(t-\Delta t)] + k_L [i_0(t+\Delta t) - i_0(t-\Delta t)]}{2\Delta t}$
Negative	$i_n(t) + k_R i_0(t)$	$u_n(t)$	$\frac{[i_n(t+\Delta t) - i_n(t-\Delta t)] + k_L [i_0(t+\Delta t) - i_0(t-\Delta t)]}{2\Delta t}$
Mode 1	$i_p(t) - i_n(t)$	$u_p(t) - u_n(t)$	$\frac{[i_p(t+\Delta t) - i_p(t-\Delta t)] - [i_n(t+\Delta t) - i_n(t-\Delta t)]}{2\Delta t}$

$di_{cal}(t)/dt$. One can observe that this equation is with 2 unknown variables of R_1 and L_1, and therefore it cannot be solved based on measurements at one time instant. Fortunately, the equation holds for all time instant after the occurrence of the fault, and therefore the redundancy of the equation is more than adequate for accurate R_1 and L_1. With $n\Delta t$ time window, rewrite (7) into the following matrix form,

$$\boldsymbol{y} = \boldsymbol{A}\boldsymbol{x} \tag{8}$$

where $\boldsymbol{y} = \begin{bmatrix} u_{cal}(t-n\Delta t) \\ \vdots \\ u_{cal}(t) \end{bmatrix}$, $\boldsymbol{A} = \begin{bmatrix} i_{cal}(t-n\Delta t) & \dfrac{di_{cal}(t-n\Delta t)}{dt} \\ \vdots & \vdots \\ i_{cal}(t) & \dfrac{di_{cal}(t)}{dt} \end{bmatrix}$, $\boldsymbol{x} = \begin{bmatrix} R_1 \\ L_1 \end{bmatrix}$,

n is the number of equations, Δt is the sampling interval, and $n\Delta t$ is the length of the time window. This is a standard state estimation problem. Here the least squares method is applied to estimate R_1 and L_1,

$$\hat{\boldsymbol{x}} = \begin{bmatrix} \hat{R}_1 & \hat{L}_1 \end{bmatrix}^T = (\boldsymbol{A}^T\boldsymbol{A})^{-1}\boldsymbol{A}^T\boldsymbol{y} \tag{9}$$

Note that $\boldsymbol{y} \in \mathbb{R}^n$, $\boldsymbol{A} \in \mathbb{R}^{n\times 2}$, and $\boldsymbol{A}^T\boldsymbol{A} \in \mathbb{R}^{2\times 2}$. For each time step, one only need to calculate several low dimensional matrix multiplications and an inverse of a 2×2 matrix. The procedure is with relatively low computational burden.

2.3.2 Protection and Faulted Pole Identification Criterion

The trip region is set as a rectangle in the *R*-*L* plane where $R_1 \in \left[-R_{margin}, R_{\max}\right]$ and $L_1 \in \left[-k_B L_B, L_{1,whole} + k_B L_B\right]$, where $L_{1,whole} = L_{s,whole} - L_{m,whole}$ is the mode 1 inductor (which is equal to the difference between the self and mutual inductor) through the whole line under protection, and L_B is the inductance value of the boundary inductor. The settings of the relay include R_{margin}, $R_{\max}$, k_B and T_{delay} (as defined at the end of the next paragraph). R_{margin} is a small positive resistance (usually tens of ohms) that can prevent mis-operation of the relay during severe internal fault near the local terminal. $R_{\max}$ is a large positive resistance to ensure dependable operation of the relay during high resistance faults. $k_B \in (0,1)$ is a constant to prevent mis-operation of the relay during internal faults close to both terminals.

The protection logic can be designed with the calculated resistance and inductance seen by the relay. Calculate $\hat{R}_1$ and $\hat{L}_1$ with quantities corresponding to the positive, negative and mode 1 options are shown in Table 1 (this procedure will result in 3 pairs of calculated $\hat{R}_1$ & $\hat{L}_1$). When there is an internal fault, at least 1 pair of the calculated results will move into the trip region. When there are external faults or system disturbances, all of the calculated results will be out of the trip region. Additionally, one can also identify the fault type by checking whether the corresponding pair of calculated $\hat{R}_1$ & $\hat{L}_1$ enters the trip region. The protection logic and fault type identification logic are shown in Table 2. Note that there are 8 possible combinations, and some of the combinations may not be meaningful (with the notation of "N/A"). To ensure security of the protection algorithm, the line is tripped when a certain pair of the calculated $\hat{R}_1$ & $\hat{L}_1$ stays in the trip region for T_{delay} period of time.

Table 2. Protection and Fault Pole Identification Logic
(√: within the trip region; ×: outside of the trip region)

Positive	Negative	Mode 1	Trip?	Faulted Pole
×	×	√	Yes	PN
√	×	×	Yes	P
×	√	×	Yes	N
√	×	√	Yes	P
×	√	√	Yes	N
√	√	×	N/A	N/A
√	√	√	Yes	PN
×	×	×	No	External

3 Results

An example ± 320kV bipolar MMC-HVDC grid is shown as Fig. 3. The length of the line of interest is 200km. The parameters of the MMC-HVDC grid and the parameters of the transmission line of interest are shown in Table 3. Faults with different types, locations and resistances are simulated in PSCAD/EMTDC. The sampling rate is selected as 100kHz, corresponding to the sampling interval of Δt=10 μs . The calculation time window is selected as $n\Delta t = 1ms$, where $n = 100$ in equation (8).

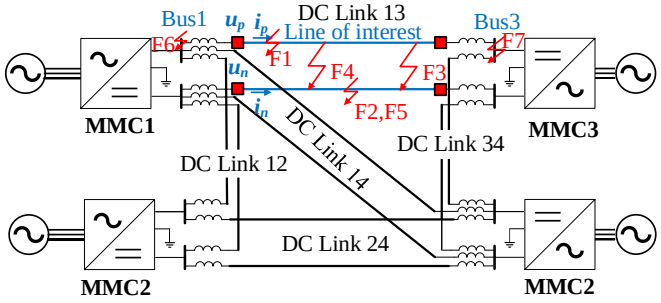

Fig.3 The topology and faults of a four terminal hybrid MMC based HVDC grid

Table 3. Parameters of the MMC-HVDC grid and the transmission line of interest

Parameters	Value
AC rated voltage (kV)	400
DC rated voltage (kV)	± 320
Self resistance (ohm/m)	1.4315e-4
Mutual resistance (ohm/m)	1.0793e-4
Self inductance(H/m)	1.3026e-5
Mutual inductance(H/m)	4.9430e-6
Boundary inductance(H)	0.1
Length of the line of interest(km)	200

The proposed distance relay is installed at the left terminal of DC Link 13, with positive and negative pole voltage and current instantaneous measurements at the local terminal. The settings of the distance relay are selected as $R_{margin} = 10ohm$, $R_{\max} = 600ohm$, $k_B = 0.3$, and $T_{delay} = 1ms$. Next, the

effectiveness of the proposed distance protection method is verified through the following 7 fault events (F_1 to F_7 as shown in Fig. 3).

3.1 Test Event 1: Internal P-G Fault with Low Fault Resistance

An internal P-G fault with 0.01ohm fault resistance occurs at 50km from the local terminal and at time t = 0.2s. The results of the proposed method are depicted in Fig. 4. The top view of the three dimensional box is also provided on the top right corner of the figure (same for the other fault events).

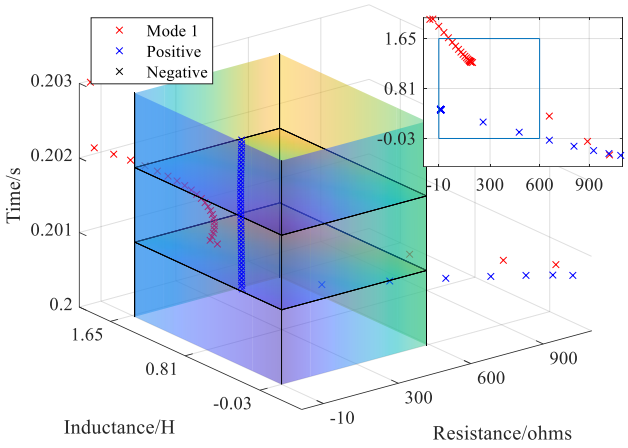

Fig. 4. Results of the proposed method for the internal 0.01ohm P-G fault at 50km and at time 0.2s

From the figure, after the fault occurs at t=0.2s, the calculated $\hat{R}_1$ & $\hat{L}_1$ corresponding to mode 1 and positive options are getting closer to the trip region. The positive option enters the trip region at t = 0.2088s and becomes stable after t=0.201s. The mode 1 option enters the trip region at t = 0.201s. However, as time goes by, mode 1 option is leaving the region rapidly, while the positive one still stays within the region. During the entire time window, the negative option stays far away from the trip region so that it is not shown in this figure. After the time delay of 1ms, the protection issues the trip signal at t = 0.202 s, and determines that the faulted pole is the positive pole according to Table 2. In the figure, the lower plane at t = 0.201s means that there are calculated resistances/inductances moving into the trip region. The upper plane at t = 0.202s means the trip signal is issued.

3.2 Test Event 2: Internal N-G Fault with Low Fault Resistance

An internal N-G fault with 0.01ohm fault resistance occurs at 100km from the local terminal and at time t = 0.2s. The results of the proposed method are depicted in Fig. 5.

It shows that only the negative option is getting closer and enters the trip region at 0.201s, and stays within the trip region. The mode 1 and positive options are both far away from the trip region. After the time delay of 1ms, the protection issues the trip signal at t = 0.202 s, and determines that the faulted pole is the negative pole according to Table 2. In the figure, the lower plane at t = 0.201s means that there are calculated resistances/inductances moving into the trip region. The upper plane at t = 0.202s means the trip signal is issued.

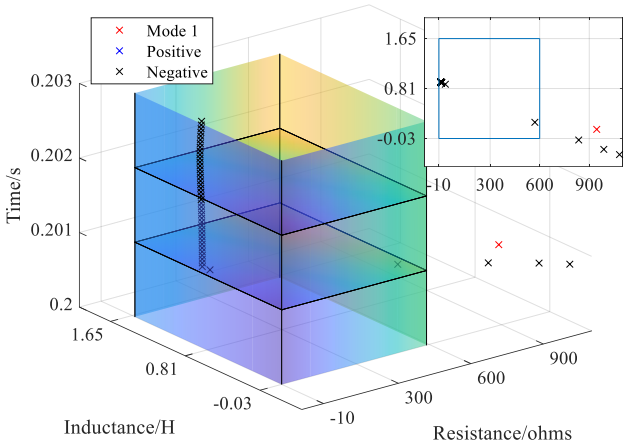

Fig. 5. Results of the proposed method for the internal 0.01ohm N-G fault at 100km and at time 0.2s

3.3 Test Event 3: Internal P-N Fault with Low Fault Resistance

An internal P-N fault with 0.01ohm fault resistance occurs at 150km from the local terminal and at time t = 0.2s. The results of the proposed method are depicted in Fig. 6.

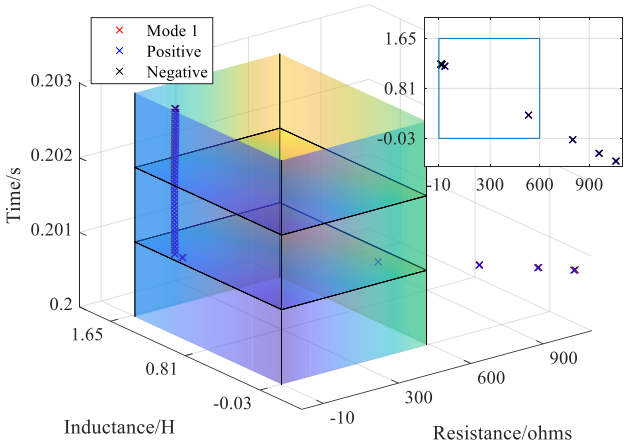

Fig. 6. Results of the proposed method for the internal 0.01ohm P-N fault at 150km and at time 0.2s

It shows that all of the three results (positive, negative and mode 1 options) are getting closer and then enter the trip region at 0.201s. The results of 3 different types are almost the same. They all stay within the trip region. After the time delay of 1ms, the protection issues the trip signal at t = 0.202 s, and determines that the faulted poles are both poles according to Table 2. In the figure, the lower plane at t = 0.201s means that there are calculated resistances/inductances moving into the trip region. The upper plane at t = 0.202s means the trip signal is issued.

3.4 Test Event 4: Internal PNG Fault with Low Fault Resistance

An internal PPG fault with 0.01ohm fault resistance occurs at 80km from the local terminal and at time t = 0.2s. The results of the proposed method are depicted in Fig. 7.

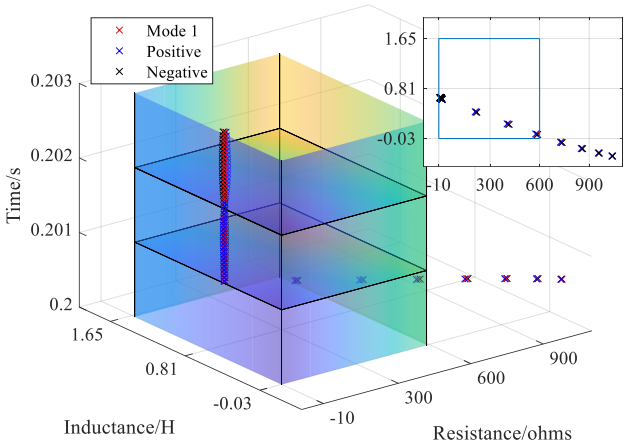

Fig. 7. Results of the proposed method for the internal 0.01ohm PPG fault at 80km and at time 0.2s

It shows that all of the three results (positive, negative and mode 1 options) are getting closer and then enter the trip region at 0.201s. The results of 3 different types are almost the same. They all stay within the trip region. After the time delay of 1ms, the protection issues the trip signal at t = 0.202 s, and determines that the faulted poles are both poles according to Table 2. In the figure, the lower plane at t = 0.201s means that there are calculated resistances/inductances moving into the trip region. The upper plane at t = 0.202s means the trip signal is issued. It also proves that for HVDC transmission lines, P-N faults are quite similar as PNG.

3.5 Test Event 5: Internal N-G Fault with High Fault Resistance

An internal N-G fault with 300ohm fault resistance occurs at 100km from the local terminal, which is also the middle of the transmission line, and at time t = 0.2s. The results of the proposed method are depicted in Fig. 8.

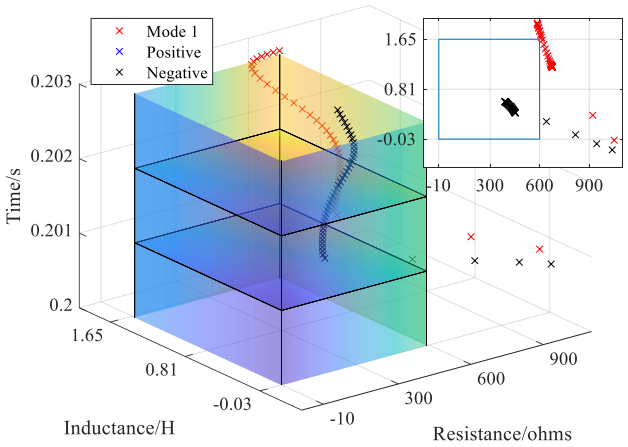

Fig. 8. Results of the proposed method for the internal 300ohm N-G fault at 100km and at time 0.2s

It shows that both the negative option and mode 1 option are getting closer to the trip region after the fault occurs at 0.2s. The positive option stays away from the region all the time. However, the negative option enters the trip region at 0.201s and stays within the region. After the time delay of 1ms, the protection issues the trip signal at t = 0.202 s, and determines that the faulted pole is the negative pole according to Table 2. In the figure, the lower plane at t = 0.201s means that there are calculated resistances/inductances moving into the trip region. The upper plane at t = 0.202s means the trip signal is issued. Comparing Fig. 8 and Fig. 5, we can easily find that high fault resistance has a great impact on the estimated results, while its results are not as stable as the low resistance one. It also shows the importance to provide proper settings of R_{max}, to ensure dependable operation during high resistance faults.

3.6 Test Event 6: External P-G Fault with Low Fault Resistance

An external P-G fault with 0.01ohm fault resistance occurs at Bus1 within the MMC converter station, which is close to the local terminal, at time t = 0.2s. The results of the proposed method are depicted in Fig. 9.

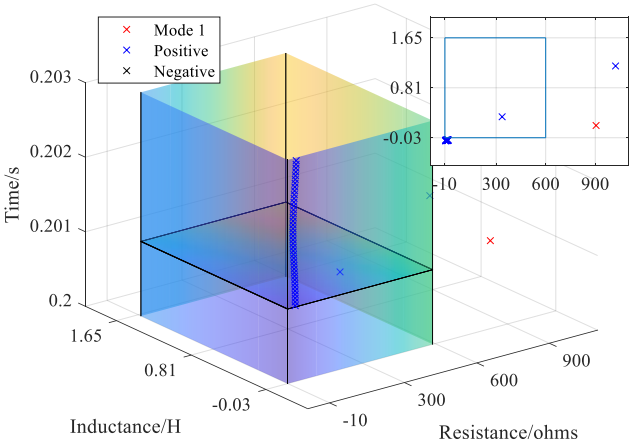

Fig. 9. Results of the proposed method for the external 0.01ohm P-G fault at Bus1 and at time 0.2s

It shows that the positive option is getting closer to the trip region and enters the trip region at 0.201s. However, it jumps out of the region immediately. Although it is close to the trip region, it still stays out of it. The mode 1 option gets close to the region at one time instant and then leaves. The negative option also stays away from the trip region. Therefore, according to Table 2, the fault is considered as an external fault. The protection securely ignores this severe external fault.

3.7 Test Event 7: External P-N Fault with Low Fault Resistance

An external P-N fault with 0.01ohm fault resistance occurs at Bus3 within the MMC converter station, which is close to the remote end of the line, at time t = 0.2s. The results of the proposed method are depicted in Fig. 10.

It shows that all of the results are getting closer to the trip region, and they enters the trip region at 0.201s, but leaves the trip region immediately. Afterwards, they all stays outside of the trip region. Therefore, according to Table 2, the fault is considered as an external fault. The protection securely ignores this severe external fault.

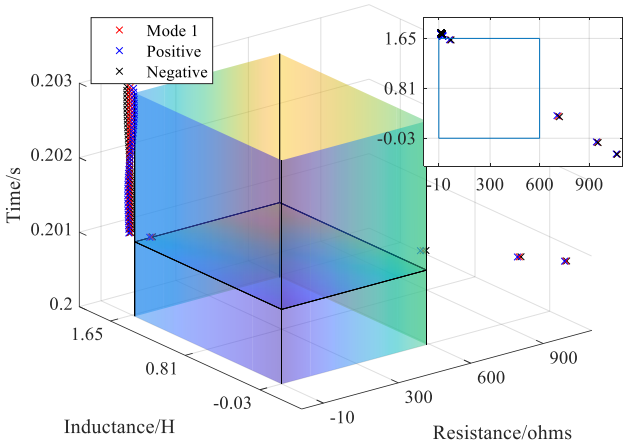

Fig. 10. Results of the proposed method for the external 0.01ohm P-N fault at Bus3 and at time 0.2s

4 Conclusion

In this paper, a novel distance protection on MMC-HVDC transmission lines is proposed. The method only requires single-ended voltage and current instantaneous measurements, without communication channels between two terminals. The method borrows the idea of legacy distance protection scheme in HVAC transmission lines, and adopts state estimation algorithm to calculate the resistance and inductance "seen" by the distance relay. Afterwards, the calculated resistance and inductance are depicted in an R-L plane to formulate the protection logic and determine the faulted poles. The complexity of the algorithm is relatively low and therefore is suitable for real-time operation of the protective relay. Simulation results prove that the proposed protection method can dependably trip internal faults (including high resistance faults) within 3 ms after the occurrence of the fault, and can securely ignore the external faults. In the future, advanced modelling methods of transmission lines could be applied, to consider distributed and frequency dependent parameter characteristics of practical DC transmission lines.

5 Acknowledgements

This work is sponsored by National Nature Science Foundation of China (No. 51807119, No. 51877135). The support is greatly appreciated.

6 References

[1] J. Liu, N. Tai and C. Fan, "Transient-Voltage-Based Protection Scheme for DC Line Faults in the Multi-terminal VSC-HVDC System," in *IEEE Transactions on Power Delivery*, vol. 32, no. 3, pp. 1483-1494, June 2017.

[2] B. Wang, Y. Liu, D. Lu, K. Yue and R. Fan, "Transmission Line Fault Location in MMC-HVDC Grids Based on Dynamic State Estimation and Gradient Descent," in *IEEE Transactions on Power Delivery*, vol. 36, no. 3, pp. 1714-1725, June 2021.

[3] T. Li, A. M. Gole and C. Zhao, "Harmonic Instability in MMC-HVDC Converters Resulting From Internal Dynamics," in *IEEE Transactions on Power Delivery*, vol. 31, no. 4, pp. 1738-1747, Aug. 2016.

[4] M. Mehrasa, E. Pouresmaeil, S. Zabihi and J. P. S. Catalão, "Dynamic Model, Control and Stability Analysis of MMC in HVDC Transmission Systems," in *IEEE Transactions on Power Delivery*, vol. 32, no. 3, pp. 1471-1482, June 2017.

[5] A. P. Meliopoulos et al., "Dynamic State Estimation-Based Protection: Status and Promise," in *IEEE Transactions on Power Delivery*, vol. 32, no. 1, pp. 320-330, Feb. 2017.

[6] Y. Liu, A. P. Meliopoulos, R. Fan, L. Sun and Z. Tan, "Dynamic State Estimation Based Protection on Series Compensated Transmission Lines," in *IEEE Transactions on Power Delivery*, vol. 32, no. 5, pp. 2199-2209, Oct. 2017.

[7] B. Gao, P. Dong, X. Liu, et al, "Research of HVDC Transmission Line Differential Under-Voltage Protection Characteristics and Value Setting," in *Power System Technology*, 2015.

[8] W. Zheng, N. Zhang, G. Yang, et al, "Comparative and improvement investigation on the DC transmission line traveling wave protections of Siemens and ABB," in Power System Protection and Control, 2015.

[9] B. Li, Y. Li, J. He, et al., "An Improved Transient Traveling-Wave Based Direction Criterion for Multi-Terminal HVDC Grid," in *IEEE Transactions on Power Delivery*, 2020.

[10] C. Zhang, G. Song, T. Wang, L. Wu and L. Yang, "Non-unit Traveling Wave Protection of HVDC Grids Using Levenberg–Marquart Optimal Approximation," in *IEEE Transactions on Power Delivery*, vol. 35, no. 5, pp. 2260-2271, Oct. 2020.

[11] J. Dong, B. Zhang, et al. "Single-ended transient-based protection for EHV transmission lines basic theory," in *Proceedings of the CSEE*, 2009.

[12] J. D, Hao. L, and Yang. L, "Non-unit Boundary Protection using Synchro-squeezing Wavelet for HVDC lines" pp. 2392-2398, *2018 International Conference on Power System Technology* (POWERCON)

[13] Y. Yang, et al., "A pilot protection scheme for HVDC transmission lines based on boundary energy." in *Proceedings of the CSEE* (2015).

[14] Y. Lei, X. He, J. Duan and H. Li, "Boundary Protection Scheme for HVDC Transmission System," *2019 IEEE 8th International Conference on Advanced Power System Automation and Protection* (APAP), 2019, pp. 75-79.

[15] S. Gao, Q. Liu, G. Song, "Current differential protection principle of HVDC transmission system". IET Generation Transmission & Distribution, 2016, 11(5):1286-1292.

[16] F. B. Costa, A. Monti, F. V. Lopes, K. M. Silva, P. Jamborsalamati and A. Sadu, "Two-Terminal Traveling-Wave Based Transmission Line Protection," in *IEEE Transactions on Power Delivery*, vol. 32, no. 3, pp. 1382-1393, June 2017.

[17] B. Wang, Y. Liu, D. Lu and X. Zheng, "MMC-HVDC Transmission Line Protection based on Bergeron Model and State Estimation", *8th IET Renewable Power Generation Conference (RPG)*, 2019.

[18] B. Li, M. Lv, B. Li, S. Xue and W. Wen, "Research on an Improved Protection Principle Based on Differential Voltage Traveling Wave for VSC-HVDC Transmission Lines," in *IEEE Transactions on Power Delivery*, vol. 35, no. 5, pp. 2319-2328, Oct. 2020.

[19] B. Wang, Y. Liu, "VSC-HVDC Transmission Line Protection Based on Dynamic State Estimation", in *IEEE Power and Energy Society General Meeting (PESGM)*, 2019.